Flux penetration into flat superconductors of arbitrary shape: Patterns of magnetic and electric fields and current

Th. Schuster, H. Kuhn, and E. H. Brandt

Max-Planck-Institut für Metallforschung, Institut für Physik, Postfach 800665, D-70506 Stuttgart, Germany
(Received 14 February 1996; revised manuscript received 29 March 1996)

The penetration of magnetic flux into flat type-II superconductors of various shapes in a perpendicular magnetic field is investigated in detail. The magnetic field distribution at the sample surface is observed by the magneto-optical Faraday effect and calculated from first principles. The investigations are performed on $DyBa_2Cu_3O_{7-\delta}$ and $YBa_2Cu_3O_{7-\delta}$ samples which were shaped into a cross or an indented rectangle by a laser-cutting technique. Magnetic and electric field and current distributions are calculated from Maxwell's equations treating the superconductor as a conductor with a highly nonlinear current-voltage law and zero reversible magnetization. A large concentration of magnetic flux and electric field and a high flux-line velocity occur at concave sample corners. This results from the fact that the flux lines can penetrate into regions of the sample which are bounded by the extensions of the sample edges only at these points. This large electric field and related energy dissipation are particularly relevant for superconducting tapes, in which ''sausaging'' effects (variations of the filament cross section) reduce their performance as an ideal conductor. Huge jumps of the electric field occur where the current flow changes from a straight to a circular path. This jump diverges as one over the distance to the corner at sharp indents or concave corners. [S0163-1829(96)04930-2]

I. INTRODUCTION

One of the most important features for applications and theoretical understanding of both conventional and high-temperature type-II superconductors is the pinning of vortices at sample inhomogeneities.[1,2] One of the parameters which characterize the pinning behavior is the critical current density j_c at which the vortices depin and start to move under the influence of the Lorentz force. This vortex drift induces an electric field E which causes a voltage drop along the specimen. Consequently, at current densities $j > j_c$ energy is dissipated and the resistivity $\rho = E/j$ becomes finite. The vortices in high-temperature superconductors (HTSC) may also depin at $j \ll j_c$ by thermal activation which is characterized by an activation energy U.

The temperature, field, and time dependences of the magnetic moment is typically determined from *integral* measurements using SQUID (superconducting quantum interference device), VSM (vibrating sample magnetometer), or torque magnetometry. Values for j_c and U which are averaged over the sample volume can be derived from such experiments.

However, *local* investigations of flux distributions in type-II superconductors by, e.g., Hall-probe measurements or magneto-optics have shown that the normal component of the magnetic induction B_z and in many cases also j and U strongly vary with the position. The spatial distribution of B_z is influenced by the sample shape,[3–10] sample thickness,[11,12] macrodefects,[13–20] surface and edge barriers,[21–27] by spatial variation of j_c,[26–28] instabilities,[29] a finite lower critical field H_{c1},[30] or the anisotropy of j_c which may be caused by the Cu-O planes,[31–35] in-plane magnetic fields,[36,37] twin boundaries,[38–44] or columnar defects that are inclined with respect to the crystal c axis.[45,46] The space-resolved methods mentioned in principle allow the determination of $j_c(B, \mathbf{r})$ and $E(j, \mathbf{r})$ even in inhomogeneous super-

conductors if appropriate evaluation methods are used. The magneto-optical technique provides a powerful tool to test these inversion methods and to verify theoretical models.

Flux penetration into type-II superconductors with flux-line pinning is well described by the Bean model[47] and its extensions[1,48–51] when the specimen is an almost infinitely extended cylinder or slab with constant j_c in a parallel magnetic field, where demagnetizing effects are negligible. The introduction of a demagnetizing factor can account for deviations from this ideal situation only in the special case of ellipsoids without pinning. However, single crystalline HTSC samples are available only as thin films or monocrystalline platelets, which are usually investigated in perpendicular magnetic field to obtain larger signals. In this geometry one has to account for large stray-field effects, and the original Bean model can be applied only to the *critical state* when the sample is completely penetrated by magnetic flux and the shielding current has reached the critical value j_c in the entire superconductor.[52] Forkl and Kronmüller[11,12] successfully used the Bean model to describe magneto-optically observed flux-density profiles at the flat surface of samples with finite thickness in the critical state. For the *partly penetrated* state the description of flux and current distributions is much more complicated. A numerical inversion method was applied to calculate the current distribution in thin circular disks[53] and squares[7–9] from measured flux density profiles.

Analytic expressions for the static magnetization and for flux and current profiles during flux penetration and exit are available for the one-dimensional (1D) perpendicular Bean model of long strips[54–56] and circular disks[57–59] and for thin strips with a geometric edge barrier.[23,60] These 1D theories of thin long strips and circular disks have recently been extended to the two-dimensional (2D) problems of thin superconductors with square, rectangular or arbitrary shape in a perpendicular field.[61–63]

Recent magneto-optical studies[10,26,27,64] demonstrated that the flux penetration and exit and flux creep are well described by model calculations using a current-voltage law of the form $E \propto (j/j_c)^n$, which conveniently interpolates between the ohmic regime of thermally activated flux flow ($n = 1$) and the classical Bean model ($n \gg 1$). Here E is the electric field and the exponent n is determined by the activation energy U. Namely, the often observed dependence $U(j) = U_c \ln(j_c/j)$ yields $E(j) = E_c \exp(-U/kT) = E_c(j/j_c)^n$ with $n = U_c/kT$. Using this model in Refs. 10 and 61 the current distribution was calculated for rectangular specimens and nice agreement with the observed cushionlike flux penetration was obtained. The electric field E was found to be maximum along the boundaries where j_c changes abruptly in samples with inhomogeneous critical-current density $j_c(\mathbf{r})$.

In this paper we show that very high electric fields inside the superconductor may be caused also by abrupt reduction *or* enlargement of the sample width. The presented magneto-optical investigation of the flux distributions in samples shaped as a cross and an indented strip in combination with the presented theory allows one to deduce the underlying current distribution and its topology.

This paper is organized as follows. A brief outline of the theoretical background and the main equations used for the calculations of magnetic and electric field and current distributions is given in Sec. II. Our magneto-optical method and sample preparation are described in Sec. III. We compare results obtained on cross-shaped samples and indented strips with theory in Sec. IV. Section V summarizes our results.

II. THEORETICAL BACKGROUND

A. Computational methods

In order to understand our magneto-optical observations of the magnetic field component B_z and to obtain the profile of the current density and electric field, we have computed all these quantities from first principles for thin superconductors of similar shapes. The details of similar such calculations may be found in Refs. 10, 61, and 62. The main idea is to derive an integral equation for a quantity which is defined only inside the superconductor, not in the entire space, and then time integrate this integral equation to obtain this quantity as a function of time. All other desired quantities in all space then follow from the Maxwell equations.

This integral equation implicitly contains the Maxwell equations $\mathbf{j} = \text{curl} \mathbf{H}$, $\dot{\mathbf{E}} = -\text{curl} \mathbf{B}$ (the dot denotes $\partial/\partial t$), and $\text{div} \mathbf{B} = 0$, the material equations $\mathbf{B} = \mathbf{B}(\mathbf{H})$ and $\mathbf{E} = \mathbf{E}(\mathbf{J})$, but also boundary conditions and the time-dependent applied field $B_a(t)$, which acts as the driving force. A formulation in terms of differential equations is less elegant since then the homogeneous applied field drops out from the equations because one has $\text{div} \mathbf{B}_a = 0$ and $\text{curl} \mathbf{B}_a = 0$ and the boundary conditions have to be considered separately.

In such computations of the flux penetration into thin superconducting strips or circular disks,[65-67] the directly calculated quantity was the sheet current $\mathbf{J}(y,z) = \int_{-d/2}^{d/2} \mathbf{j}(x,y,z) dz$, which in these simplest geometries has only one component and depends on only one variable, namely, $\mathbf{J} = \hat{\mathbf{y}} J(x)$ or $\mathbf{J} = \hat{\varphi} J(r)$.

For all other flat geometries $\mathbf{J}(x,y)$ has x and y components and depends on x and y. However, since $\text{div} \mathbf{J} = 0$ holds

in the absence of current sources, one may define a scalar ''local magnetization'' or ''density of current loops'' $g(x,y)$ by writing

$$\mathbf{J}(x,y) = -\hat{\mathbf{z}} \times \nabla g(x,y) = \nabla \times \hat{\mathbf{z}} g(x,y), \quad (1)$$

and requiring that $g = 0$ on the edge of the specimen. The resulting integral equation for g,

$$\dot{g}(x,y,t) = \mathcal{F}\{g(x',y',t), \dot{B}_a(t)\}, \quad (2)$$

was time-integrated for homogeneous superconductors of square and rectangular cross sections in Refs. 10, 61, and 62. In the present paper we apply this solution method to thin samples of more complicated shape, which in addition may exhibit inhomogeneous critical current density $j_c(x,y)$. As stated above, we assume $\mathbf{B} = \mu_0 \mathbf{H}$ and $\mathbf{E} = \rho \mathbf{j}$ with nonlinear isotropic (scalar) resistivity $\rho(j) = \rho_c(j/j_c)^{n-1}$, equivalent to $\rho(J) = \rho_c(J/J_c)^{n-1}$ with $J_c = j_c d$.

B. Nonrectangular superconductors

Our numerical program, originally developed for rectangular films, may be applied to films of arbitrary shape as follows.

One may simulate, e.g., a cross-shaped (or circular, star, ring-shaped, etc.) specimen by considering a square specimen which has $J_c = 1$ inside the cross-shaped region and $J_c \ll 1$ in the ''free space'' outside the cross but still inside the square. This square with inhomogeneous resistivity behaves almost like a cut-out cross except that a weak current can flow in the cut-out region. This current cannot be made arbitrarily small since the required high resistivity $\rho = \rho_c(J/J_c)^{n-1}$ requires very small time steps during time-integration of our integral equation (2).

Alternatively, one may use a different method which is much faster and avoids the unphysical current outside the nonrectangular specimen. Namely, we multiply at each time step the function $g(x,y)$ by a function $C(x,y)$ which is unity inside the specimen and zero outside the specimen. This ''cutting function'' suppresses the current outside the specimen. The method is mathematically correct since it modifies the integral kernel $Q(\mathbf{r}, \mathbf{r}')$ which relates the local field $H(\mathbf{r})$ to the function $g(\mathbf{r})$ by

$$H(\mathbf{r}) = \int d^2r' Q(\mathbf{r}, \mathbf{r}') g(\mathbf{r}') + H_a, \quad (3)$$

such that the integration is over the physical specimen only rather than over the total square. This allows us to use the kernel $Q(\mathbf{r}, \mathbf{r}')$ calculated for the rectangular specimen by a Fourier method.[61] The $\mathbf{r}_i$, $g(\mathbf{r}_i)$, and $H(\mathbf{r}_i)$ are vectors and $Q(\mathbf{r}_i, \mathbf{r}_j)$ is a large matrix of up to 900×900 elements in our computation if the discrete $\mathbf{r}_i$ are chosen on a 30×30 grid covering one quarter of the rectangular specimen, or one eighth of the square, due to symmetry.

This second computational method is fast and stable. However, it produces unphysical spatial oscillations of $J(x,y)$ and $E(x,y)$ if the cut-out of the cross is sharp and the number of grid points inside the cross is not large. These oscillations were partly suppressed by choosing a smooth cutting function which continuously goes from 1 to 0 over a few grid spacings. This smoothing simulates the finite thick-
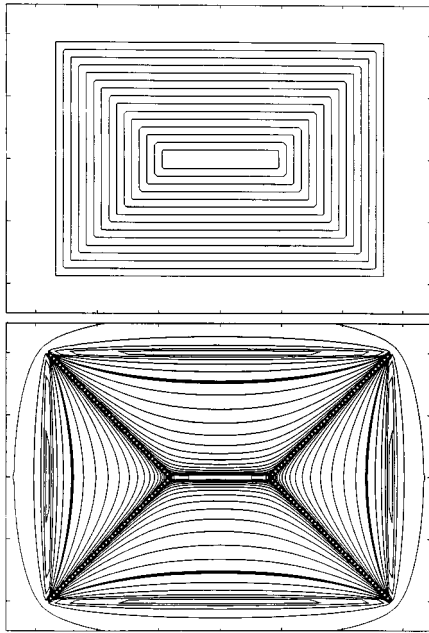
FIG. 1. Top: stream lines of the current in a thin type-II super-conductor of rectangular shape in the critical state. Bottom: normal component of the magnetic field as a contour plot.

ness of the specimen and broadens the infinite peak in the electric field $E(x,y)$ which occurs at the four concave corners of the cross as discussed in Sec. IV. However, care has to be taken in this second method that the obtained current density or function $g(x,y)$ is sufficiently accurate to yield exactly $H(\mathbf{r})=0$ in the nonpenetrated regions; cf. Eq. (3). This condition $H=0$ is a very sensitive criterion for the numerical accuracy in the Bean-like case ($n\gg1$).

To facilitate the understanding of the complicated current and field patterns in the investigated samples we will give in the following a brief summary of the topology of current and field distributions of rectangular samples in the fully penetrated critical state. A detailed discussion of the critical state in thin superconductors is published in Ref. 52.

C. Critical state in rectangular superconductors

Our computation reproduces the results of the Bean model for the particular choices $J_c(H)=$ const and $n\gg1$. The current density takes its maximum possible value $|\mathbf{j}|=j_c$ in the entire specimen if the sample is in the critical state, i.e., fully penetrated by magnetic flux. In addition, the current density has to satisfy the continuity condition $\mathrm{div}\mathbf{j}=0$ and has to flow parallel to the surfaces. It follows from these conditions that the current stream lines have sharp bends in superconductors with rectangular cross section; this is a characteristic feature of vector fields with constant modulus.[68] These sharp bends form discontinuity lines (d lines) which divide the superconductor into domains with uniform parallel current flow as discussed in the review by Campbell and Evetts;[1] see the upper plot in Fig. 1. One distinguishes two types of d lines:[52] At d^+ lines the orientation of $\mathbf{j}_c$ changes discontinuously but the magnitude of j_c remains the same. At d^- lines the magnitude of j_c changes, e.g., at the specimen surface or at inner boundaries where regions of different j_c meet. The

current stream lines have to bend sharply in the critical state in order to satisfy the condition of continuous current flow at such boundaries. The d^+ lines run along the bisection lines starting from the sample corners and on a section of the central line parallel to the longer side as shown in the lower plot in Fig. 1, when the superconductor is isotropic in the x-y plane.

Characteristic features of the d^+ and d^- lines are the following.

(1) Whereas the d^- lines occur at internal and external boundaries of the sample (local sample geometry), the d^+ lines form in homogeneous regions and are determined by the shape of the sample.

(2) Flux lines cannot cross the d^+ lines since during increase or decrease of the applied magnetic field the flux motion is directed towards or away from the d^+ lines, respectively. In contrast, the d^- lines can be crossed by moving flux lines, e.g., when flux lines penetrate from the surface. When the current does not flow parallel to the d^- line, a strong flux motion is directed along the d^- line.

(3) The electric field E is largest at the d^- lines, whereas we have $E=0$ at the d^+ lines.[10,62]

(4) The d^+ and the d^- lines do not change their position during lowering or reversal of the external magnetic field, although the magneto-optically detected intensities of the d^+ and d^- lines are reversed in the remanent state.

The d^+ and d^- lines are clearly seen in thin type-II superconductors (thickness $\ll$ lateral extension) because of the logarithmic infinity of B_z at the sample surface.[52]

D. Electric field during flux penetration

If the (linear or nonlinear) resistivity is isotropic in the x-y plane, then the current stream lines coincide with the field lines of the electric field $\mathbf{E}$ inside the superconductor. In particular, the field lines of $\mathbf{E}(x,y)$ like those of $\mathbf{J}(x,y)$ are equidistant lines in the Bean model with constant j_c namely, straight parallel lines or concentric circles. The penetrating fronts of $H(x,y)$ and $E(x,y)$ coincide in the partly penetrated state and are composed of straight lines and circles surrounding the flux-free region in which both $H=0$ and $E=0$. One has also $J=0$ in this region in the longitudinal geometry, but $J(x,y)$ is finite over the entire area of the specimen in perpendicular geometry.[55,57] However, since $J(x,y)<J_c$ in the flux-free region, one has $E(x,y)=0$ in this region because of the factor $(J/J_c)^n$ with $n\gg1$ in $E(J)$. The orientation of $\mathbf{E}(x,y)$ is thus fixed by the shape of the superconductor and of the penetrating flux front.

We give now a very general estimate of the electric field induced during field increase in superconductors of arbitrary cross section in longitudinal and perpendicular geometries. First we note that the local derivative $\partial B_z(x,y,t)/\partial t=-\hat{\mathbf{z}}(\nabla\times\mathbf{E})$ is not too much different from the ramp rate of the applied field, $\partial B_a/\partial t=\dot{B}_a$. This assumption is even exact in longitudinal geometry in the approximation $\mathbf{B}=\mu_0\mathbf{H}$ (or $B_{c1}=0$). It is a good approximation in perpendicular geometry, where it is violated most at the penetrating flux front. $\dot{B}(x,y)=\dot{B}_a$ applies exactly for arbitrary specimen shape and field orientation in the fully penetrated Bean critical state.

The electric field $\mathbf{E}(x,y)$ in the critical state is known in principle if the specimen shape is known. It has to satisfy the induction law $\nabla\times\mathbf{E}(x,y)=-\hat{\mathbf{z}}\dot{B}_a$ and its orientation is predicted by topology. In regions with straight parallel stream lines the general solution of this equation is ($\hat{\mathbf{x}}$, $\hat{\mathbf{y}}$, and $\hat{\mathbf{z}}$ are unit vectors)

$$\mathbf{E}(x,y)=[(\dot{B}_a+c)y+f(x)]\hat{\mathbf{x}}+[cx+g(y)]\hat{\mathbf{y}}, \quad (4)$$

where c is an arbitrary constant and $f(x)$ and $g(y)$ are arbitrary functions. One easily verifies that Eq. (4) satisfies $\partial E_y/\partial x-\partial E_x/\partial y=-\dot{B}_a$.

In particular, in regions where J flows along $\hat{\mathbf{x}}$ one has

$$\mathbf{E}=E\hat{\mathbf{x}}, \quad E(x,y)=\dot{B}_a y+f(x). \quad (5)$$

Electric field patterns $|\mathbf{E}(x,y)|$ of this type are depicted in Ref. 62 for rectangular superconductors, where they look like an inverted roof or like a folded cardboard.

In general the surfaces $|\mathbf{E}(x,y)|$ may also be curved, namely, when $f(x)$ is a nonlinear function; this occurs when not all discontinuity lines are straight lines, e.g., a parabola which separates regions of straight and circular current flow.

In regions where the stream lines form concentric circles, the general solution for $\mathbf{E}(r,\varphi)$ is

$$\mathbf{E}(r,\varphi)=\frac{1}{2}\dot{B}_a\left[\frac{r_p^2(\varphi)}{r}-r\right]\hat{\boldsymbol{\varphi}}. \quad (6)$$

Here r and φ are polar coordinates centered at the center of the circles, $\hat{\boldsymbol{\varphi}}=(-y\hat{\mathbf{x}}+x\hat{\mathbf{y}})/r$ is the unit vector along φ, and $r_p(\varphi)$ is an arbitrary function which has the meaning of a penetration radius. Equation (6) applies for $r\leq r_p(\varphi)$ where the brackets in Eq. (6) are ≥ 0. For $r\geq r_p(\varphi)$ one has $E=0$ if the line $r=r(\varphi)$ is the flux front; else E takes one of the forms (4) or (6) but with different center of the circles. The midpoint of the circles coincides with the center or point of a defect in the otherwise homogeneous superconductor, e.g., a circular hole or a round or sharp notch in the specimen edge. The sharper such a defect is the higher is the $1/r$ peak of E in Eq. (6).

The expressions (4) and (6) are exact for $\mathbf{E}$ in the fully penetrated critical state in both longitudinal and perpendicular geometries, and in longitudinal geometry also for partial penetration, and they should be a good approximation also in the partly penetrated state of films of arbitrary shape. This expectation is confirmed by our computations of flux penetration into cross-shaped or indented superconducting platelets.

III. EXPERIMENTS

A. Faraday effect

We visualize the magnetic field distribution of a superconductor by magneto-optics. Since the HTSC themselves have no significant magneto-optical effect, the sample surfaces have to be covered by a magneto-optically active material. For our investigations we use the magneto-optical Faraday effect. The flux penetration is imaged by detecting the rotation of the polarization plane when linearly polarized light passes a magneto-optically active layer exposed to the magnetic field of the underlying superconductor. The light is

reflected from flux-free regions without rotation of the polarization plane; this light thus cannot pass an analyzer which is set in a crossed position with respect to the polarizer. Thus the Shubnikov phase (with a flux-line lattice) will be imaged as bright areas, whereas the flux-free Meissner phase remains dark. We used ferrimagnetic iron-garnet films with an in-plane anisotropy as magneto-optical indicators for the experiments presented in this paper.

The iron garnet film was grown by liquid phase epitaxy onto a gallium-gadolinium substrate with a thickness of about 3.5 μm (commercial firm Gamma Scientific Production, Russia).[69] This kind of indicator allows the flux penetration into HTSC samples to be observed directly in the whole temperature regime of superconductivity with a magnetic sensitivity of about 1 mT and a spatial resolution of about 4 μm. The indicator was glued directly onto the sample surface with a conductive carbon cement. The finite thickness and a possible spacing between indicator and sample leads to a smearing of the observed flux distributions.[27]

The external magnetic field is generated by a copper solenoid coil, which is cooled with liquid nitrogen and produces a maximum field of 0.55 T. The observations were performed in the optical cryostat described in Refs. 70 and 71. The field can be changed at different constant ramp rates. Since the sample is subject to flux creep during the experiment, different ramp rates lead to different flux penetration depths at the same value of the applied field.[72] The basic consideration of flux, current and electric field distributions in thin superconductors are not affected by this phenomenon.

B. Sample preparation

We use DyBa$_2$Cu$_3$O$_{7-\delta}$ (DBCO) single crystals prepared as described in Ref. 73 and YBa$_2$Cu$_3$O$_{7-\delta}$ (YBCO) single crystals which were prepared at the Universität Karlsruhe, Germany, by the method described in Ref. 74. The crystal dimensions are about $1000\times1000\times15$ μm^3 and $T_c\approx 88$ K (DBCO) and $T_c\approx 92$ K (YBCO) as measured by the Meissner effect using SQUID magnetometry. All crystals have a distinct twin structure which was revealed by polarized light microscopy.

The samples were patterned at the Institut für Strahlwerkzeuge, Universität Stuttgart, using the laser micromachining technique described in Ref. 75. As shown in Ref. 75 the laser cutting does not influence the superconducting parameters of the sample.

IV. RESULTS AND DISCUSSION

A. Cross

To point out the excellent qualitative agreement between theory and experiment we compare calculated distributions of the normal field component H_z with magneto-optically determined flux patterns for various sample shapes.

The left column in Fig. 2 shows the calculated current pattern in a cross for different flux-penetration depths. The density of the stream lines gives the magnitude of the current density. The current stream line outside the cross in the upper left plot is caused by the finite critical current density there; cf. Sec. II B. The contour plots of the corresponding
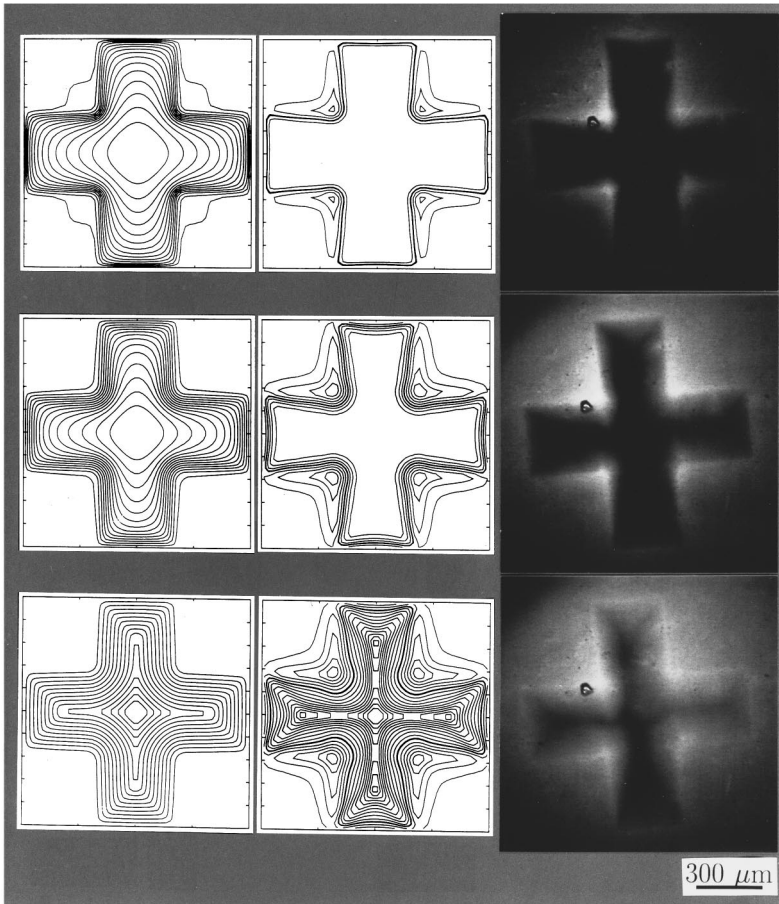
FIG. 2. Calculated current pattern (left column) and perpendicular field H_z (middle column) of a cross-shaped sample at three different times during flux penetration in increasing H_a. Right column: magneto-optically observed flux distributions in cross-shaped DBCO crystal at $T=20$ K and $\mu_0 H_a=41$ mT (top), 82 mT (middle), and 123 mT (bottom), detected using a ferrimagnetic iron-garnet indicator. The black spot is a defect in the indicator film. The crystal thickness is $d=15$ μm. In the calculations the unit of the magnetic field (one fit parameter) is chosen such that best agreement is found with the observed flux distributions.

field distributions are plotted in the middle column. The right column shows magneto-optically detected flux distributions in a thin DBCO single crystal for the three different perpendicular external magnetic fields $\mu_0 H_a=41$ mT (top row), 82 mT (middle row), and 123 mT (bottom row); the same H_a values were used in the theory. The experiments were carried out at $T=20$ K using a ferrimagnetic iron-garnet indicator. The white areas correspond to the Shubnikov-Phase, into which the flux lines have already penetrated, whereas the flux-free Meissner phase remains dark. The observed flux distributions are slightly disturbed due to the influence of the twin boundaries. The black spot on the right arm of the cross is a defect in the iron-garnet indicator.

The shielding currents flow in the *whole* sample in our perpendicular geometry to ensure $B_z=0$ in the Meissner area, in contrast to the longitudinal geometry, where the shielding currents flow only in the penetrated regions. Comparing the current distributions depicted for the three magnetic fields one finds that during magnetization the shielding currents change their magnitude and their direction until the critical value j_c is reached. The current flows parallel to the sample edges at places where the shielding current has reached j_c. But a direction parallel to the sample edges is no longer defined at the *concave* corners of the cross.

Next we address the question of the current flow in the region that is bounded by the extrapolation of the sample edges. Two alternatives are conceivable at first thought as depicted in Fig. 3 for a cross-shaped sample. We assume the cross to be in the critical state to avoid the problems arising

from the above discussed changes in the direction and magnitude of the currents. The d^+ lines are plotted as bold lines, the arrows indicate the direction of the current flow. In the first possibility shown in the upper plot, the current streamlines are extended beyond the concave corner and meet at an angle of 90° such that a d^+ line must be formed along the bisection line. In the second possibility the streamlines run on concentric circles around the corner as shown in the lower plot in Fig. 3. No d^+ line is formed in this latter case and the electric field, Eq. (6), and vortex velocity have a $1/r$ peak. Our magneto-optical experiments in Fig. 2 clearly reveal that the flux front runs smoothly around the concave corners. Consequently a d^+ line is not visible. We conclude from these observations that the latter possibility is realized. The calculations in Fig. 2 show also that the current and the flux front run on smooth curves around the concave corner and thus nicely agree with the experiment and the above consideration.

What consequences does this behavior imply? The circular current stream lines induce a high magnetic field peak in the center of the circles, i.e., at the concave corners. This is also visible in the magneto-optic images and in the calculated contour plots of the magnetic field in Fig. 2. The flux lines which penetrate the region bounded by the central d^+ lines and the dashed lines in Fig. 4 have to pass through the concave corner of the cross since the flux line motion is directed always perpendicular to the current flow as indicated by the dashed arrows. ''Flux jets'' occur at the concave corners, i.e., the flux-line velocity and therefore the electric field are very large.[52]
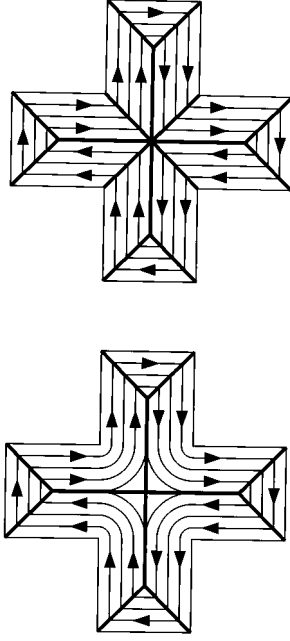
FIG. 3. Sketch of the current streamlines in a cross-shaped sample in the critical state. Upper plot: the streamlines meet at 90° at the concave corner and a d^+ line is formed. Lower plot: the streamlines run on concentric circles around the concave corner.

The stream lines of the current and contour plots of the magnetic field in the fully penetrated critical state are depicted in Fig. 5 with particularly high resolution for a cross with arms half as wide as long, using a grid of 60×60 points and prescribing the current distribution with the highest attainable accuracy using our computation of flux penetration.

We give here the explicit expression for the electric field $E(x,y)$ inside the superconductor near the lower left concave corner of the cross, if flux-creep effects are neglected and E depends only on the ramp rate of the applied magnetic field. We shift the origin of the x and y axes into this corner
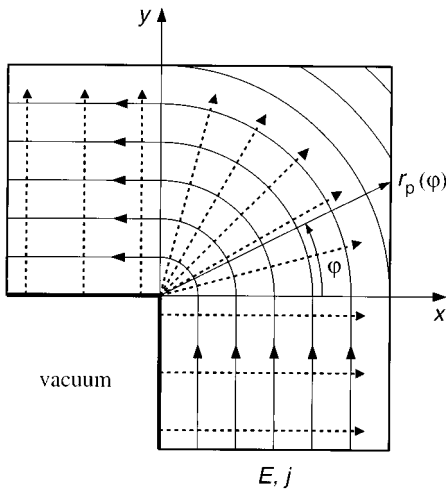
FIG. 4. Current flow and flux-line motion at one concave corner of a cross-shaped sample. The direction of the current is indicated by the arrows along the streamlines; the direction of flux-line motion is indicated by the arrows perpendicular to the current stream lines.
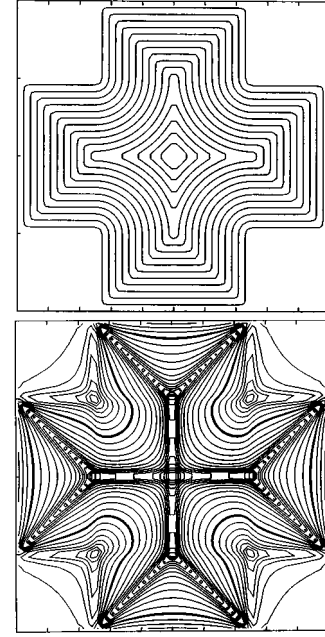
FIG. 5. Stream lines of the current (top) and contour plots of the magnetic field (bottom) in the fully penetrated critical state of a cross with arms half as wide as long.

for convenience (see Fig. 4) and define $r=(x^2+y^2)^{1/2}$, $\hat{\varphi}=(-y\hat{\mathbf{x}}+x\hat{\mathbf{y}})/r=\hat{\mathbf{z}}\times\hat{\mathbf{r}}$. When the flux front has penetrated to a depth r_p, the electric field caused by the ramp rate $\dot{B}_a$ is obtained from Eqs. (4) and (6) and from the condition $E=0$ at this front. Explicitly one has

$$\mathbf{j}=+j_c\hat{\mathbf{y}}, \quad \mathbf{E}=\dot{B}_a(R-x)\hat{\mathbf{y}}, \quad x>0, \ y<0, \qquad (7a)$$

$$\mathbf{j}=+j_c\hat{\varphi}, \quad \mathbf{E}=\frac{\dot{B}_a}{2}\left(\frac{r_p^2}{r}-r\right)\hat{\varphi}, \quad x>0, \ y>0, \qquad (7b)$$

$$\mathbf{j}=-j_c\hat{\mathbf{x}}, \quad \mathbf{E}=\dot{B}_a(y-R)\hat{\mathbf{x}}, \quad x<0, \ y>0. \qquad (7c)$$

The streamlines of $\mathbf{j}$ and $\mathbf{E}$ flow around this corner smoothly as depicted in Fig. 4. However, while the current density is a continuous vector field with constant magnitude $|\mathbf{j}|=j_c$ and with no jumps in its components j_x and j_y, the electric field exhibits pronounced *discontinuities* on the x and y axes, i.e., on the extension of the corner sides into the superconductor. Namely, on the line $y=0$, $x>0$ one has $E_x=0$, $E_y=(x-r_p)\dot{B}_a$ at $y<0$, and $E_x=0$, $E_y=(x/2)(1-r_p^2/r)\dot{B}_a$ at $y>0$, and corresponding behavior on the line $x=0$, $y>0$. This means that at the positions where the straight stream lines start to curve into circles, the magnitude of E performs a jump. For example, E_y jumps by

$$\delta E_y=\dot{B}_a\frac{(r_p-x)^2}{2x} \qquad (8)$$

at $y=0$. This jump height diverges at the corner as $1/x$ and corresponds to an electric surface charge of density δE_y caused by the motion of the flux lines.

We have thus the remarkable result that during flux penetration into the corner a surface charge, and a corresponding abrupt jump in the electric field, appear *inside* the supercon-

ductor along the lines (or planes) which extrapolate the edges into the specimen. Note that this discontinuity occurs at positions where the material is homogeneous and where the current flow is smooth.

This interesting phenomenon is described by Eqs. (7) and (8) in the Bean limit in longitudinal geometry. However, as discussed in Sec. II D, that description approximately applies also to perpendicular geometry with partial or full penetration of flux. The expressions for $E(x,y)$ are identical for longitudinal and perpendicular geometries in the fully penetrated critical state. A slight modification is then required in Eq. (7), which is still valid in the quarter with circular flow if the constant penetration depth r_p is replaced by a penetration radius $r_p(\varphi)$ which depends on the angle φ. Namely, if the width of the arms of the cross is $2r_0$, one has $r_p = r_0$ in the sectors of straight parallel flow, and $r_p = r_0/\max(\cos\varphi,\sin\varphi)$ since the flux front now coincides with the two central lines (planes) of the cross.

As noted by Indenbom[76] a jump in $E(x,y)$ may occur in even simpler geometries, e.g., whenever a *convex* corner is rounded. The simplest case[76] is the rectangle with rounded ends ("football stadium"), where regions with straight parallel and circular stream lines border on each other, creating a jump of E_x by a factor of 2. This can be seen from the explicit expressions $E = \pm\dot{B}_a y\hat{\mathbf{x}}$ and $E = (1/2)\dot{B}_a r\hat{\varphi}$ in these two regions; cf. Eqs. (4) to (6) with $f(x)=0$ and $r_p(\varphi)=0$ and appropriate definitions of r and φ. While this jump is finite and increases linearly with r, the jump of E near *concave* corners diverges as $1/r$ and thus becomes *infinite* when the corner is ideally sharp.

When flux creep is taken into account, i.e., when $n<\infty$ is chosen in our model $E = E_c(j/j_c)^n\mathrm{sgn}j$, then these considerations still apply if $n \gg 1$. The current density in the fully penetrated regions now is no longer exactly constant, since we have $j = j_c(E/E_c)^{1/n}\mathrm{sgn}E$. The jumps in E thus lead to small jumps in j of relative height $\delta j/j_c \approx (1/n)\delta E/(\dot{B}_a r_p)$, or with Eq. (8),

$$\delta j \approx j_c \frac{(r_p-x)^2}{2nr_px}, \qquad (9)$$

where x is the distance from the corner. These jumps in E and j are, however, smeared out due to the finite exponent n. This means an abrupt jump in j never occurs.

These considerations are confirmed by our numerical calculations. Three-dimensional plots of the electric field are shown in Fig. 6 for the same applied magnetic fields as in Fig. 2. The E-field distributions were calculated numerically using the "cutting function" as described in Sec. II B. The sharp peaks due to the large flux-line velocity and the concentration of the magnetic field at the concave corners are clearly visible. The electric field is maximum at the d^- lines along the sample edges, whereas we have $E=0$ at the flux front, along the d^+ lines, and in the Meissner phase. In the computations of Fig. 6 the number of independent grid points (points in one quarter section) was $n_x \times n_y = 30 \times 30$, and the arms of the cross were $2 \times 13 = 26$ grid points wide. This relatively small number of grid points in these arms together with the artificial smearing of the boundaries of the cross required to suppress oscillations, caused a smearing of the abrupt jump of E predicted by Eq. (9).
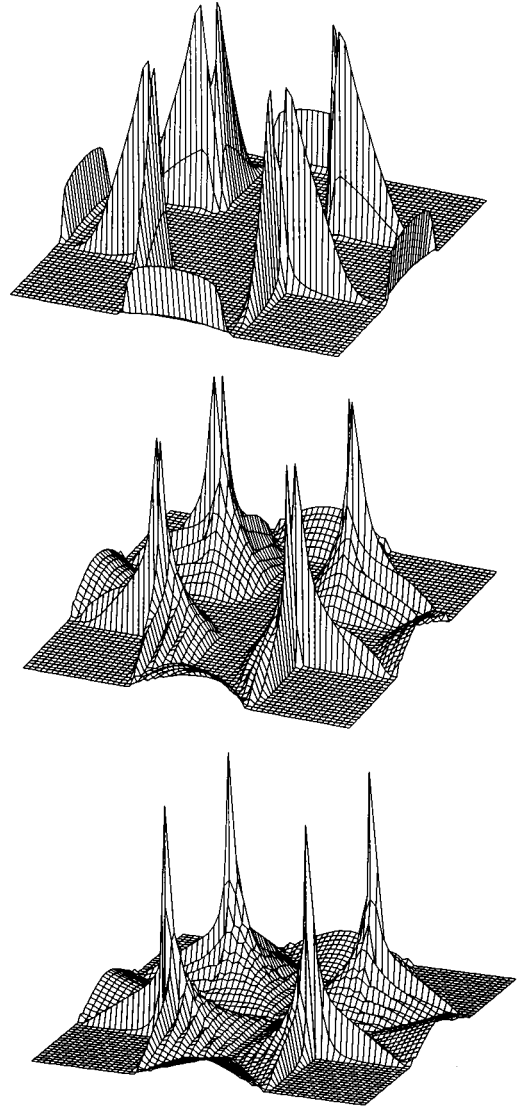
FIG. 6. Calculated magnitude $|\mathbf{E}(x,y)|$ of the electric field during flux penetration into a thin superconductor cross at applied field values (from top to bottom) 0.1, 0.3, 1.2 in units of the field of full penetration. A total of 60×60 grid points and a current-voltage law $E \propto J^9$ were used.

The $1/r$ dependence of the electric field in the region of circular flow is nicely confirmed by our computations. Figure 7 shows profiles of $E(x,y)$ taken along a straight diagonal line starting at a concave corner of the cross where $r=0$ by definition. Figure 7 was extracted from the same computer run as Fig. 6. The solid curve in Fig. 7 should be given by Eq. (7b), which in the fully saturated Bean state contains no fit parameter. However, since the position of the $1/r$ singularity (the concave corner) is not known exactly due to our artificial smearing of the boundaries of the cross, we had to use r_p as a fit parameter. The resulting curve $E(r)$, Eq. (7b), closely fits all 13 points obtained from our computation. Similar good fits to the $E = (\dot{B}_a/2)(r - r_p^2/r)$ behavior are obtained for the partly penetrated state. Fewer grid points with $E>0$ are available in this case, but still only one fit parameter r_p is required to obtain good agreement. If the amplitudes of both terms in E ($\propto r$ and $\propto 1/r$) are fitted, the
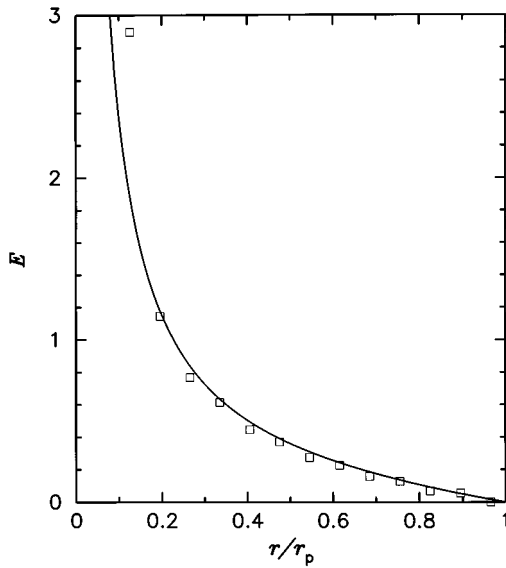
FIG. 7. Calculated profiles of the electric field along the diagonal from the concave corner to the sample center in the fully penetrated state. The boxes mark the calculated values at the grid points; the solid curve is computed from Eq. (7b).

prefactor of the r term turns out to be close to $\dot{B}_a/2$, which indicates that Eqs. (7) are a good approximation even for the partly penetrated state in perpendicular geometry.

B. Indented rectangle

The $1/r$ peak of the electric field is cut off when the concave corner is rounded. To demonstrate this we cut two semicircular indents into a rectangular ($b/a=1.07$) YBCO

platelet by laser machining. From the above arguments we expect that the magnetic and electric fields should exhibit a large overshoot at the indents. Figure 8 shows the calculated current (left) and magnetic field (middle) pattern which correspond to the magneto-optically observed flux distributions at $T = 20$ K and $\mu_0 H_a = 27$ mT, 82 mT, and 123 mT (from top to bottom) depicted in the right column. The current and field patterns were computed using a cutting function which suppresses the current flow outside the specimen; see Sec. II B. The magneto-optic images show the expected large enhancement of the magnetic field at the indents. The critical current flows parallel to the sample edges in the fully penetrated critical state. Then, additionally to the d^+-line structure in a rectangular sample discussed in Sec. II C, new parabolic d^+ lines occur where the straight current flow turns sharply into the circular path around the indents.[52] The poorer visibility of the parabolic d^+ lines compared to the others is due to the decrease of their intensity with $\cos\alpha/2$, when α is the angle by which the stream lines bend. This angle increases along the d^+ lines such that their visibility decreases. The current in the sample center is undercritical in the partly penetrated state and does not exhibit sharp bends such that a d-line structure is less visible. Note the nice agreement between the calculated and the experimental flux patterns.

Computed electric field profiles $|\mathbf{E}(x,y)|$ are depicted in Fig. 9. They are cut off at a height 5 (in units $a\dot{B}_a$) since plotting the full peak (of height ≈ 300) would have made invisible the rooflike profiles of height $\lesssim 1$ near the specimen edges. The sharp front of the penetrating electric field and the nearly circular cross section of the peak are clearly visible.
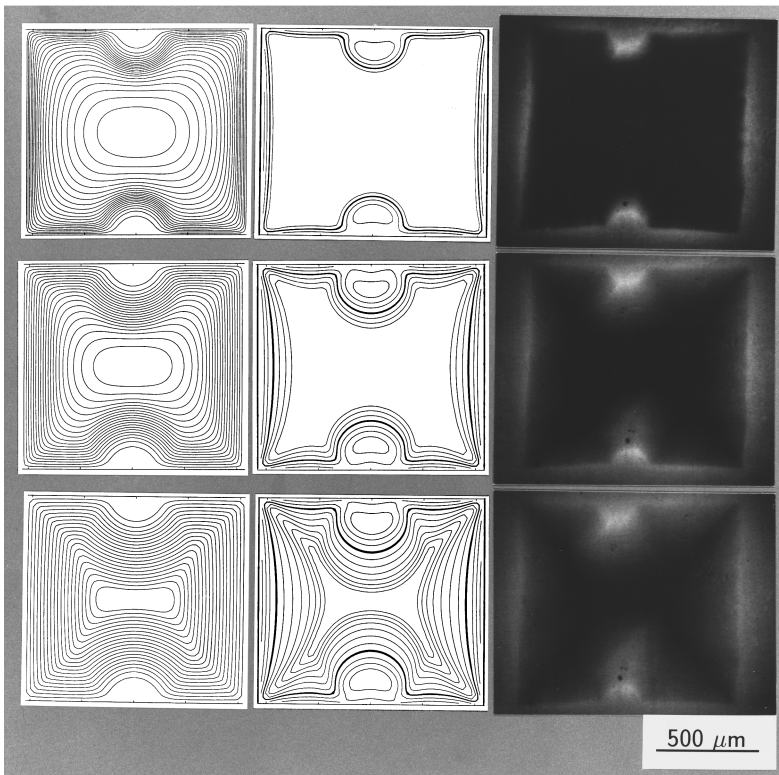
FIG. 8. Calculated current pattern (left column) and perpendicular field H_z (middle column) distribution of an indented rectangular sample for three different steps of flux penetration. Right column: magneto-optically detected flux distributions in a rectangular YBCO crystal with two semi-circular indents at $T=20$ K and $\mu_0 H_a=27$ mT (top), 62 mT (middle), and 123 mT (bottom). The flux distributions were detected using a ferrimagnetic iron-garnet indicator. The black spots are defects in the indicator film. The crystal thickness is $d=20$ μm. In the calculations the unit of the magnetic field (one fit parameter) is chosen such that best agreement is found with the observed flux distributions.
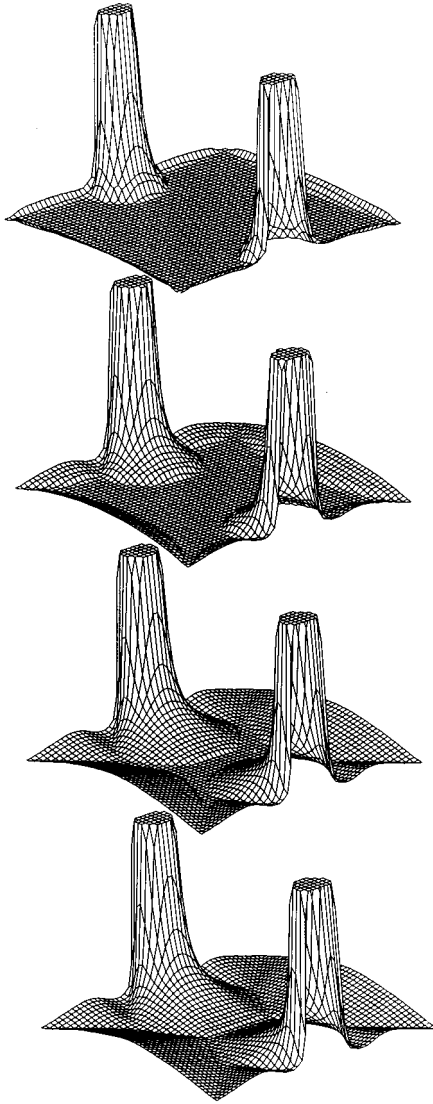
FIG. 9. Calculated magnitude $|\mathbf{E}(x,y)|$ of the electric field during flux penetration into the same superconductors with two semicircular indents as in Fig. 8. The profiles correspond to applied field values 0.15, 0.3, 0.6, and 1.05 in units of the field of full penetration; the first three field values coincide with those in Fig. 8. To make visible the entire structure we have cut the peaks of the depicted 3D plots at a height of 5 in units $a\dot{B}_a$, where a is the half width of the rectangle. The full peak height is approximately 300.

Figure 10 shows cross sections of $E(x,0)$ along the line connecting the two indents (the y axis). The fitted solid curves were chosen in the form of Eq. (7b), with $r=x_0-x$ where x_0 is the (fitted) center of the indent. Full penetration corresponds to $x=0$, or $r=x_0$. The specimen half width a (along x) was chosen as unit length in this figure. Depicted are the cases $h_a = 0.1$, 0.3, 0.6, and 1.05 in units of the field of full penetration. The function $E=(\dot{B}_a/2)(r-r_p^2/r)$ is a good fit for full penetration, where only the peak position x_0 was adjusted since $r_p=a-x_0$ is known in this case. For partial penetration also the penetration radius r_p and the prefactor $\leqslant\dot{B}_a/2$ had to be adjusted to get good fits.
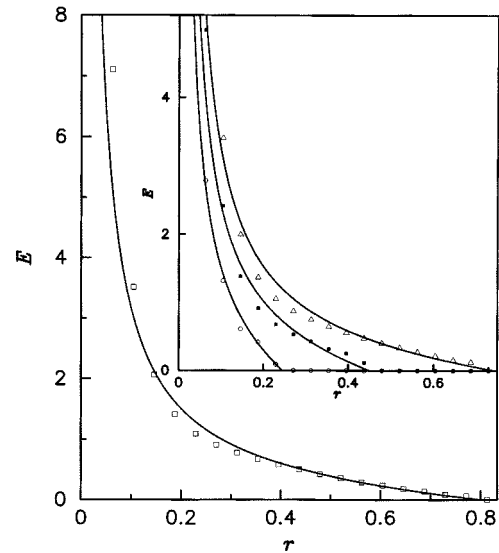
FIG. 10. Calculated profiles of the electric field along the narrowest cross section of the indented rectangle for four different magnetic fields. The symbols mark the calculated values at the grid points; the solid curves are computed from Eq. (7b). ($\square$) fully penetrated state. The inset shows the profiles for the same field values as Fig. 8.

V. CONCLUSION

In this paper we have presented patterns of electric and magnetic fields and current during penetration of flux into flat type-II superconductors which were shaped as a cross or an indented rectangle by a laser-cutting method. The magneto-optically observed flux distributions show that the magnetic field is peaked at the concave sample corners. This finding coincides with our numerical calculations of magnetic field patterns. The current flows along circular paths around the concave corners and causes large peaks of the magnetic field there. With the knowledge of the d-line formation at convex corners and the behavior of the current flow and the resulting electric and magnetic fields at concave corners the current and electric and magnetic field patterns can be derived for any arbitrary planar geometry.

Analytical solutions of the electric field E were found for long samples with cross section of arbitrary shape in a longitudinal applied magnetic field. These solutions are also valid for thin samples in perpendicular magnetic field in the fully penetrated state and they are good approximations in the partly penetrated state of thin superconductors.

The electric field pattern at convex and concave corners differ qualitatively: Discontinuity lines are formed at the convex corners where the straight field lines of j and E bend sharply and where $|E|$ goes linearly to zero. The field lines of j and E are circular around concave corners, and E diverges at the corner tip as one over the radius of the circle.

When the current flow changes from a straight to a circular path the electric field performs abrupt jumps. Note that this jump now occurs at positions where there is no inhomogeneity in the sample. Similar jumps of E occur also in inhomogeneous superconductors at positions where the critical current density changes, as observed and discussed in Ref.

10. The jump height diverges as $1/r$ at concave corners and is infinite when the corner is sharp. Our numerical calculations of the electric field distribution nicely agree with our analytical expressions.

These results are particularly important for the performance of superconductors in high-current and high-field applications because the large electric fields at concave corners or indents along the conductors may trigger flux jumps and thus lead to thermal instabilities.

In this paper we have avoided any statements about the electric field outside the specimen, and we have not considered multiply connected superconductors, e.g., plates with a rectangular hole. These are two separate and nontrivial problems, which require more specifications, e.g., the knowledge of the shape of the coil generating the applied magnetic field, or the pinning strength of the flux lines parallel to the flat surface which may limit the peak of the Meissner screening current at the inner edge of a perforated thin superconductor. Work on these topics is in progress.

[1] A. M. Campbell and J. E. Evetts, *Critical Currents in Superconductors* (Taylor & Francis, London, 1972).

[2] G. Blatter, M. V. Feigel'man, V. B. Geshkenbein, A. I. Larkin, and V. M. Vinokur, Rev. Mod. Phys. **66**, 1125 (1994).

[3] R. P. Huebener, V. A. Rowe, and R. T. Kampwirth, J. Appl. Phys. **41**, 2963 (1970).

[4] V. K. Vlasko-Vlasov, M. V. Indenbom, V. I. Nikitenko, A. A. Polyanskii, R. L. Prozorov, I. V. Grekhov, L. A. Delimova, I. A. Liniichuk, A. V. Antonov, and M. Yu. Gusev, Superconductivity **5**(9), 1582 (1992).

[5] P. Brüll, D. Kirchgässner, and P. Leiderer, Physica (Amsterdam) C **182**, 339 (1991).

[6] Th. Schuster, M. Leghissa, M. R. Koblischka, H. Kuhn, H. Kronmüller, and G. Saemann-Ischenko, Physica (Amsterdam) C **203**, 203 (1992).

[7] P. D. Grant, M. W. Denhoff, W. Xing, P. Brown, S. Govorkov, J. C. Irwin, B. Heinrich, H. Zhou, A. A. Fife, and A. R. Cragg, Physica (Amsterdam) C **229**, 289 (1994).

[8] W. Xing, B. Heinrich, H. Zhou, A. A. Fife, and A. R. Cragg, J. Appl. Phys. **76**, 4244 (1994).

[9] D. Reinel, W. Dietrich, A. Majhofer, and T. Wolf, Physica (Amsterdam) C **245**, 193 (1995).

[10] Th. Schuster, H. Kuhn, E. H. Brandt, M. V. Indenbom, M. Kläser, G. Müller-Vogt, H.-U. Habermeier, H. Kronmüller, and A. Forkl, Phys. Rev. B **52**, 10 375 (1995).

[11] A. Forkl and H. Kronmüller, Physica (Amsterdam) C **228**, 1 (1994).

[12] A. Forkl and H. Kronmüller, Phys. Rev. B **52**, 16 130 (1995).

[13] Th. Schuster, M. R. Koblischka, H. Kuhn, H. Kronmüller, G. Friedl, B. Roas, and L. Schultz, Appl. Phys. Lett. **62**, 768 (1993).

[14] M. R. Koblischka, Th. Schuster, and H. Kronmüller, Physica (Amsterdam) C **211**, 263 (1993).

[15] M. R. Koblischka, Th. Schuster, and H. Kronmüller, Physica (Amsterdam) C **219**, 205 (1994).

[16] V. K. Vlasko-Vlasov, V. N. Goncharov, V. I. Nikitenko, A. A. Polyanskii, I. F. Voloshin, L. M. Fisher, N. M. Aleshina, and O. A. Poluschenko, Physica (Amsterdam) C **222**, 367 (1994).

[17] U. Welp, D. O. Gunter, G. W. Crabtree, W. L. Carter, V. K. Vlasko-Vlasov, and V. I. Nikitenko, Appl. Phys. Lett. **66**, 1270 (1995).

[18] U. Welp, D. O. Gunter, G. W. Crabtree, W. Zhong, U. Balachandran, P. Haldar, R. S. Sokolowski, V. K. Vlasko-Vlasov, and V. I. Nikitenko, Nature **376**, 44 (1995).

[19] R. Hedderich, Th. Schuster, H. Kuhn, J. Geerk, G. Linker, and M. Murakami, Appl. Phys. Lett. **66**, 3215 (1995).

[20] A. E. Pashitski, A. Polyanskii, A. Gurevich, J. A. Parrell, D. C. Larbalestier, Physica (Amsterdam) **246**, 133 (1995).

[21] M. V. Indenbom, H. Kronmüller, T. W. Li, P. H. Kes, and A. A. Menovsky, Physica (Amsterdam) C **222**, 203 (1994).

[22] L. A. Dorosinskii, V. I. Nikitenko, and A. A. Polyanskii, Phys. Rev. B **50**, 501 (1994); L. A. Dorosinskii, K. Reber, and A. Hubert, Physica (Amsterdam) C **256**, 319 (1996).

[23] E. Zeldov, A. I. Larkin, V. B. Geshkenbein, M. Konczykowski, D. Majer, B. Khaykovich, V. M. Vinokur, and H. Shtrikman, Phys. Rev. Lett. **73**, 1428 (1994).

[24] E. Zeldov, D. Majer, M. Konczykowski, A. I. Larkin, V. M. Vinokur, V. B. Geshkenbein, V. M. Vinokur, N. Chikumoto, and H. Shtrikman, Europhys. Lett. **30**, 367 (1995).

[25] D. Majer, E. Zeldov, and M. Konczykowski, Phys. Rev. Lett. **75**, 1166 (1995).

[26] Th. Schuster, M. V. Indenbom, H. Kuhn, E. H. Brandt, and M. Konczykowski, Phys. Rev. Lett. **73**, 1424 (1994).

[27] Th. Schuster, H. Kuhn, E. H. Brandt, M. Indenbom, M. R. Koblischka, and M. Konczykowski, Phys. Rev. B **50**, 16 684 (1994).

[28] B. Khaykovich, E. Zeldov, M. Konczykowski, D. Majer, A. I. Larkin, and J. R. Clem, Physica (Amsterdam) C **235-240**, 2757 (1994).

[29] V. K. Vlasko-Vlasov, V. I. Nikitenko, A. A. Polyanskii, G. W. Crabtree, U. Welp, and B. W. Veal, Physica (Amsterdam) C **222**, 361 (1994).

[30] M. V. Indenbom, Th. Schuster, H. Kuhn, H. Kronmüller, T. W. Li, and A. A. Menovsky, Phys. Rev. B **51**, 15 484 (1995).

[31] A. A. Polyanskii, L. A. Dorosinskii, M. V. Indenbom, V. I. Nikitenko, Yu. A. Osipyan, and V. K. Vlasko-Vlasov, J. Less-Common Met. **164&165**, 1300 (1990).

[32] S. Gotoh and N. Koshizuka, Physica (Amsterdam) C **176**, 300 (1991).

[33] Th. Schuster, M. R. Koblischka, H. Kuhn, M. Glücker, B. Lude-

scher, and H. Kronmüller, J. Appl. Phys. **74**, 3307 (1993).

[34] C. A. Durán, P. L. Gammel, R. Wolfe, V. J. Fratello, D. J. Bishop, T. Kimura, K. Kitazawa, and K. Kishio, Phys. Rev. B **49**, 3608 (1994).

[35] E. Cuche, M. V. Indenbom, M.-O. André, P. Richard, W. Benoit, and Th. Wolf, Physica (Amsterdam) C **256**, 324 (1996).

[36] M. V. Indenbom, A. Forkl, B. Ludescher, H. Kronmüller, H.-U. Habermeier, B. Leibold, G. D'Anna, T. W. Li, P. H. Kes, and A. A. Menovsky, Physica (Amsterdam) C **226**, 325 (1994).

[37] Th. Schuster, H. Kuhn, and M. V. Indenbom, Phys. Rev. B **52**, 15621 (1995).

[38] Th. Schuster, M. R. Koblischka, B. Ludescher, and H. Kronmüller, J. Appl. Phys. **72**, 1478 (1992).

[39] A. I. Belyaeva, S. V. Voitsenya, V. P. Yur'ev, M. A. Obolenskii, and A. V. Bondarenko, Superconductivity **5**, 1406 (1992).

[40] C. A. Duran, P. L. Gammel, R. Wolf, V. J. Fratello, D. J. Bishop, J. P. Rice, and D. M. Ginsberg, Nature **357**, 474 (1992).

[41] V. K. Vlasko-Vlasov, M. V. Indenbom, and A. A. Polyanskii, in *The Real Structure of High-T_c Superconductors*, edited by V. Sh. Shekhtman, Springer Series in Materials Science Vol. 23 (Springer, Berlin, Heidelberg, 1993), pp. 111–144.

[42] A. I. Belyaeva, S. V. Voitsenya, V. P. Yuriyev, M. A. Obolenskii, and A. V. Bondarenko, Solid State Commun. **55**, 427 (1993).

[43] M. Turchinskaya, D. L. Kaiser, F. M. Gayle, A. J. Shapiro, A. Roytburd, V. Vlasko-Vlasov, A. Polyanskii, and V. Nikitenko, Physica (Amsterdam) C **216**, 205 (1993).

[44] V. K. Vlasko-Vlasov, L. A. Dorosinski, A. A. Polyanskii, V. I. Nikitenko, U. Welp, B. W. Veal, and G. W. Crabtree, Phys. Rev. Lett. **72**, 3246 (1995).

[45] Th. Schuster, M. V. Indenbom, H. Kuhn, H. Kronmüller, M. Leghissa, and G. Kreiselmeyer, Phys. Rev. B **50**, 9499 (1994).

[46] Th. Schuster, H. Kuhn, M. Indenbom, M. Leghissa, M. Kraus, and M. Konczykowski, Phys. Rev. B **51**, 16 358 (1995).

[47] C. P. Bean, Phys. Rev. Lett. **8**, 250 (1962); Rev. Mod. Phys. **36**, 31 (1964); J. Appl. Phys. **41**, 2482 (1970).

[48] V. M. Krasnov, V. A. Larkin, and V. V. Ryazanov, Physica (Amsterdam) C **174**, 440 (1991).

[49] S. Senoussi, J. Phys. III (Paris) **2**, 1041 (1992).

[50] M. E. McHenry and R. A. Sutton, Prog. Mater. Sci. **38**, 159 (1994).

[51] K. V. Bhagwat and P. Chaddah, Physica (Amsterdam) C **224**, 155 (1994).

[52] Th. Schuster, M. V. Indenbom, M. R. Koblischka, H. Kuhn, and H. Kronmüller, Phys. Rev. B **49**, 3443 (1994).

[53] H. Theuss, A. Forkl, and H. Kronmüller, Physica (Amsterdam) C **190**, 345 (1992).

[54] W. T. Norris, J. Phys. D: Appl. Phys. **3**, 489 (1970); Y. Young, T. Hughes, C. Beduz, D. M. Spiller, R. G. Scurlock, and W. T. Norris, Physica (Amsterdam) C **256**, 378 (1996).

[55] E. H. Brandt, M. Indenbom, and A. Forkl, Europhys. Lett. **22**, 735 (1993); E. H. Brandt and M. Indenbom, Phys. Rev. B **48**, 12 893 (1993).

[56] E. Zeldov, J. R. Clem, M. McElfresh, and M. Darwin, Phys. Rev. B **49**, 9802 (1994).

[57] P. N. Mikheenko and Yu. E. Kuzovlev, Physica (Amsterdam) C **204**, 229 (1993).

[58] J. Zhu, J. Mester, J. Lockhart, and J. Turneaure, Physica (Amsterdam) C **212**, 216 (1993).

[59] J. R. Clem and A. Sanchez, Phys. Rev. B **50**, 9355 (1994).

[60] M. Benkraouda and J. R. Clem, Phys. Rev. B **53**, 5716 (1996); J. R. Clem, R. P. Huebener, and D. E. Gallus, J. Low Temp. Phys. **5**, 449 (1973); W. Buck, K.-P. Selig, and J. Parisi, *ibid.* **45**, 21 (1981); J. Provost, E. Paumier, and A. Fortini, J. Phys. F **4**, 439 (1974); I. L. Maksimov and A. A. Elistratov, Pis'ma Zh. Éksp. Teor. Fiz. **61**, 204 (1995) [Sov. Phys. JETP Lett. **61**, 208 (1995)].

[61] E. H. Brandt, Phys. Rev. Lett. **74**, 3025 (1995).

[62] E. H. Brandt, Phys. Rev. B **52**, 15442 (1995).

[63] E. H. Brandt, Rep. Prog. Phys. **58**, 1465 (1995).

[64] Th. Schuster, H. Kuhn, and E. H. Brandt, Phys. Rev. B **51**, 697 (1995).

[65] E. H. Brandt, Phys. Rev. B **49**, 9024 (1994).

[66] E. H. Brandt, Phys. Rev. B **50**, 4034 (1994).

[67] E. H. Brandt, Physica (Amsterdam) C **235-240**, 2939 (1994).

[68] H. A. M. van den Berg, J. Appl. Phys. **60**, 1104 (1986).

[69] L. A. Dorosinskii, M. V. Indenbom, V. I. Nikitenko, Yu. A. Ossip'yan, A. A. Polyanskii, and V. K. Vlasko-Vlasov, Physica (Amsterdam) C **203**, 149 (1992).

[70] Th. Schuster, M. R. Koblischka, N. Moser, B. Ludescher, and H. Kronmüller, Cryogenics **31**, 811 (1991).

[71] K.-H. Greubel, E. Gmelin, N. Moser, Ch. Mensing, and L. Walz, Cryogenics **30** (Suppl.), 457 (1990).

[72] M. R. Koblischka and R. J. Wijngaarden, Supercond. Sci. Technol. **8**, 199 (1995).

[73] C. Thomsen, M. Cardona, B. Gegenheimer, R. Liu, and R. Simon, Phys. Rev. B **37**, 9860 (1988).

[74] A. Erb, T. Traulsen, and G. Müller-Vogt, J. Cryst. Growth **137**, 487 (1994).

[75] Th. Schuster, H. Kuhn, A. Raiber, T. Abeln, F. Dausinger, H. Hügel, M. Kläser, and G. Müller-Vogt, Appl. Phys. Lett. **68**, 2568 (1996).

[76] M. V. Indenbom (private communication).